Transition state geometry in radical abstraction reactions: comparison of interatomic distances in the intersecting parabolas and Morse curves models with quantum-chemical calculations

A. F. Shestakov and E. T. Denisov★

Institute of Problems of Chemical Physics, Russian Academy of Sciences,
14 Institutskii prosp., 142432 Chernogolovka, Moscow Region, Russian Federation.
Fax: +7 (096) 524 9676. E-mail: edenisov@icp.ac.ru

Interatomic distances in the transition state were estimated for the reactions of radical abstraction: $H^{\bullet} + H_2$, $H^{\bullet} + HCl$, $H^{\bullet} + CH_4$, $N^{\bullet}H_2 + NH_3$, $HO^{\bullet} + H_2O$, $HO_2^{\bullet} + HOOH$, and $C^{\bullet}H_3 + SiH_4$. The calculation was performed by the quantum-chemical density functional method or coupled clusters method (QCH), as well as by the methods of intersecting parabolas (IPM) and Morse curves (IMM), using experimental data (activation energies and reaction enthalpies). The results of the latter two methods are close to the quantum-chemical calculation and differ only by the increment a: r(IPM or IMM) = $a + r$(QCH), where $a = -4.5 \cdot 10^{-12}$ m for IPM and $a = +1.9 \cdot 10^{-12}$ m for IMM.

Key words: quantum chemistry, interatomic distance, density functional method, intersecting parabolas method, intersecting Morse curves method, free radical abstraction reaction, transition state geometry.

The intersecting parabolas model (IPM) makes it possible to estimate the bond elongation in the transition state and to calculate interatomic distances in the reaction site using experimental data (enthalpy and activation energy of the reaction).[1—3] The same goal can be reached using the intersecting Morse curves model (IMM).[4] In turn, the modern quantum-chemical methods allow one to calculate both the geometry and the energy of the transition state for various radical reactions. The results of such calculations can be considered rather reliable, especially for the systems with a limited number of atoms. In our previous work,[5] we compared the results of the IPM and density functional (B3LYP) calculations for the radical abstraction reaction

$$CH_3C^{\bullet}H_2 + C_2H_6 \longrightarrow C_2H_6 + CH_3C^{\bullet}H_2$$

and revealed that the C—H distances in the transition state found in both approaches were very close.

This work is devoted to the systematic study of this problem using various radical abstraction reactions. The following reactions were chosen for the study:

$$H^{\bullet} + H_2 \longrightarrow H_2 + H^{\bullet},$$

$$H^{\bullet} + HCl \longrightarrow H_2 + Cl^{\bullet},$$

$$H^{\bullet} + CH_4 \longrightarrow H_2 + C^{\bullet}H_3,$$

$$N^{\bullet}H_2 + NH_3 \longrightarrow NH_3 + N^{\bullet}H_2,$$

$$HO^{\bullet} + HOH \longrightarrow HOH + HO^{\bullet},$$

$$HO_2^{\bullet} + HOOH \longrightarrow HOOH + HO_2^{\bullet},$$

$$C^{\bullet}H_3 + SiH_4 \longrightarrow CH_4 + Si^{\bullet}H_3.$$

The obtained experimental data were examined in the framework of two semiempirical models: IPM and IMM. The quantum-chemical calculations were performed by the hybrid density functional method B3LYP and, in particular cases, by the MP4 and CCSD methods using the extended 6-311++G(d,p) basis set and GAUSSIAN 98 program.[6]

Calculation methods and results

Intersecting parabolas method.[1—3] In this method, the transition state of the abstraction reaction of the type

$$B^{\bullet} + HA \longrightarrow BH + A^{\bullet}$$

is considered as an intersection point of two parabolas in the bond elongation Δr—bond energy U coordinates

$$U_{AH} = -D_{AH} + (b\Delta r_{AH})^2. \quad (1)$$

Parabola (1) describes the stretching vibration of the attacked A—H bond, and the stretching vibration of the formed B—H bond is described by another parabola

$$U_{BH} = -D_{BH} + (b_f\Delta r_{BH})^2. \quad (2)$$

Published in Russian in *Izvestiya Akademii Nauk. Seriya Khimicheskaya,* No. 2, pp. 306—315, February, 2003.

1066-5285/03/5202-320 $25.00

Table 1. Parameters of radical abstraction reactions in the IPM and IMM models[1–4]

Reaction	$b \cdot 10^{-11}$ /kJ$^{1/2}$ mol$^{-1/2}$ m^{-1}	α	$0.5hLv_i$ /kJ mol^{-1}	log(A/L mol^{-1} s^{-1})	D_e(A—H) /kJ mol^{-1}
$H^{\cdot} + H_2 \rightarrow H_2 + H^{\cdot}$	4.153	1.000	26.2	10.15	462.2
$H^{\cdot} + HCl \rightarrow H_2 + Cl^{\cdot}$	3.937	0.948	17.9	10.00	449.2
$H^{\cdot} + CH_4 \rightarrow H_2 + C^{\cdot}H_3$	3.743	0.901	17.4	11.30	457.4
$C^{\cdot}H_3 + CH_4 \rightarrow CH_4 + C^{\cdot}H_3$	3.743	1.000	17.4	8.90	457.4
$N^{\cdot}H_2 + NH_3 \rightarrow NH_3 + N^{\cdot}H_2$	4.306	1.000	20.0	8.48	469.4
$HO^{\cdot} + H_2O \rightarrow H_2O + HO^{\cdot}$	4.749	1.000	21.8	8.30	519.8
$HO_2^{\cdot} + HOOH \rightarrow HOOH + HO_2^{\cdot}$	4.600	1.000	21.2	8.00	390.2
$C^{\cdot}H_3 + SiH_4 \rightarrow CH_4 + Si^{\cdot}H_3$	2.756	0.736	12.6	8.90	400.0

Each reaction is characterized by the following parameters:

1) enthalpy ΔH_e, which includes the zero-point energy of the reacting bonds ($\Delta H_e = D_{AH} - D_{BH} + 0.5hL(\nu_{AH} - \nu_{BH})$), where ν_{AH} and ν_{BH} are the frequencies of stretching vibrations of the corresponding bonds;

2) energy barrier E_e, which includes the experimentally measured activation energy E and the additive equal to the zero-point energy of the cleaved bond ($E_e = E + 0.5hL\nu_{AH} - 0.5RT$);

3) coefficient $b = 2\pi\nu_{AH}\sqrt{\mu_{AH}}$ ($2b^2$ is the force constant of the attacked A—H bond);

4) coefficient α ($\alpha = \nu_{AH}/\sqrt{\mu_{AH}}\,/(\nu_{BH}\sqrt{\mu_{AH}})$);

5) parameter r_e (overall elongation of the A—H and B—H bonds in the transition state).

The geometry of the A...H...B transition state is characterized by two distances: r_{A-H} and r_{B-H}. The first of them is calculated by the formula

$$r_{A-H} = r_{AH} + \sqrt{E_e}/b, \qquad (3)$$

where r_{AH} is the equilibrium distance between the A and H atoms in the AH molecule.

The second distance is calculated using the formula

$$r_{B-H} = r_{BH} + \alpha\sqrt{E_e - \Delta H_e}/b, \qquad (4)$$

where r_{BH} is the equilibrium distance between the B and H atoms, and $2(b/\alpha)^2$ is the force constant of the B—H bond in the BH molecule. The overall elongation of the A—H and B—H bonds in the transition state is

$$r_e = b^{-1}(\sqrt{E_e} + \alpha\sqrt{E_e - \Delta H_e}), \qquad (5)$$

and the A—B distance in the transition state is the following:

$$r_{A-B} = r_{AH} + r_{BH} + r_e. \qquad (6)$$

The α, b, and $0.5hL\nu_{AH}$ parameters and pre-exponential factors A (averaged experimental A values) are presented in Table 1. The bond lengths for the molecules involved in the considered reactions are presented in Table 2.[7]

The initial experimental data (averaged over the results of measurements of the activation energy E) and the calculated r_e, r_{A-H}, and r_{B-H} values are presented in Table 3. The r_e values show that the bonds in the transition state are elongated by 0.3—0.5 Å, which is 14—24% of the bond lengths in the initial molecules.

Intersecting Morse curves model.[4] This model considers the transition state of the radical abstraction reaction as a result of intersection of two Morse curves. One Morse curve characterizes the potential energy of the cleaved bond (A—H), and another Morse curve characterizes that of the formed (B—H) bond as a function of the elongation of this bond. Each curve also depends only on two parameters: the energy of bond dissociation D_{ei} and coefficient b (see above) determining the force constant of the bond. The reaction, as in IPM, is characterized by the activation energy E_e and enthalpy ΔH_e (see above). The length of the cleaved A—H bond in the transition state is calculated using the formula

$$r_{A-H} = r_{AH} + \frac{\sqrt{D_{eAH}}}{b_{AH}} \ln \frac{\sqrt{D_{eAH}}}{\sqrt{D_{eAH}} - \sqrt{E_e}}. \qquad (7)$$

The length of the formed B—H bond is calculated from the formula

$$r_{B-H} = r_{BH} + \frac{\sqrt{D_{eBH}}}{b_{BH}} \ln \frac{\sqrt{D_{eBH}}}{\sqrt{D_{eBH}} - \sqrt{E_e - \Delta H_e}}. \qquad (8)$$

The overall elongation of the bonds in the transition state r_e is calculated using the formula

$$r_e = \frac{\sqrt{D_{eAH}}}{b_{AH}} \ln \frac{\sqrt{D_{eAH}}}{\sqrt{D_{eAH}} - \sqrt{E_e}} + \frac{\sqrt{D_{eBH}}}{b_{BH}} \ln \frac{\sqrt{D_{eBH}}}{\sqrt{D_{eBH}} - \sqrt{E_e - \Delta H_e}}. \qquad (9)$$

The total A...H...B bond length is calculated from formula (6).

Table 2. Bond lengths in molecules involved in the reactions under study

Molecule	Bond	$r \cdot 10^{10}$/m
H_2	H—H	0.746
HCl	H—Cl	1.274
CH_4	C—H	1.059
NH_3	N—H	1.009
H_2O	O—H	0.958
H_2O_2	O—H	0.970
SiH_4	Si—H	1.570

Table 3. Geometric parameters of the reactions ($A^{\bullet} + HB \rightarrow AH + B^{\bullet}$) calculated by the IPM and IMM methods using experimental data

Reaction	E /kJ mol^{-1}	Bond	IPM		IMM		Refs.
			$r_e \cdot 10^{11}$	$r_{A-H} \cdot 10^{11}$	$r_e \cdot 10^{11}$	$r_{A-H} \cdot 10^{11}$	
			m				
$H^{\bullet} + H_2$	29.0±2.4	H—H	3.54	9.23	4.34	9.63	8—12
$H^{\bullet} + HCl$	14.5±0.5	H—Cl	3.02	14.16	3.56	14.39	13—17
		H—H		9.06		9.37	
$H^{\bullet} + CH_4$	56.0±5.2	C—H	4.38	12.86	5.61	13.48	11, 18—23
		H—H		9.57		10.18	
$C^{\bullet}H_3 + CH_4$	58.6±4.2	C—H	4.62	13.00	5.92	13.55	11, 23, 24
$N^{\bullet}H_2 + NH_3$	61.3	N—H	4.19	12.18	5.42	12.80	11
$HO^{\bullet} + H_2O$	18.4	O—H	2.63	10.59	3.08	11.12	25
$HOO^{\bullet} + HOOH$	23.1	O—H	2.85	11.13	3.47	11.43	3
$C^{\bullet}H_3 + SiH_4$	29.4±0.2	Si—H	4.90	18.02	6.35	18.49	23, 26—29
		C—H		13.17		14.14	

The results of calculation of r_e, r_{A-H}, and r_{B-H} from the experimental data (enthalpies and activation energies) are presented in Table 3. These data are close to the values calculated in the framework of the IPM model.

Quantum-chemical calculations. To calculate the energy barriers and the geometry of transition states of the reactions under study, we used the hybrid B3LYP density functional method, which has proved to be valid for these purposes.[30—32] The results of calculation using the extended 6-311++G(d,p) basis set are presented in Table 4. However, it turned out that this approach strongly underestimated the activation energy of the $H^{\bullet}$ + HCl and $HO^{\bullet}$ + H_2O reactions. The tendency to underestimating the activation barriers in the B3LYP approach has already been noticed.[32,33] Therefore, additional calculations were performed for these systems with taking into account more carefully the correlation energy on the basis of the MP4/6-311++G** and CCSD/6-311++G** approaches (see Table 4). The test CCSD(T)/6-311++G** calculations for the $H^{\bullet}$ + HCl system gave the results almost identical to those of the CCSD/6-311++G** approach.

In general, taking into account the correlation effects according to the perturbation theory or the coupled clusters method gives close results for both the activation barrier and the geometry of the initial and transition states. However, in the case of the $HO^{\bullet}$ + HOH system, the lowest transition state with the C_2 symmetry turns out to be a minimum in the MP4 approach, although its geometry differs slightly from that found by the CCSD method. Contrary to what has been expected, the reactions with the symmetric transition state

$$N^{\bullet}H_2 + NH_3 \longrightarrow NH_3 + N^{\bullet}H_2,$$

$$HO^{\bullet} + HOH \longrightarrow HOH + HO^{\bullet},$$

$$HOO^{\bullet} + HOOH \longrightarrow HOOH + HO_2^{\bullet}$$

are characterized by the nonlinear geometry of the O—H—O and N—H—N fragments in the transition state. Therefore, the higher lying transition states of a higher order with the linear A—H—A fragments were localized (see Table 4). The increase in the energy for them is not very significant, especially for the $HOO^{\bullet}$ + HOOH reaction.

Previously, in order to elucidate the physical sense of the r_e parameter obtained by the IPM method for the $C_2H_5^{\bullet}$ + H—C_2H_5 system, the cross section of the potential energy surface in the vicinity of the transition state was calculated for the hydrogen atom displacements along the H—C and C—H line (angle C—H—C is equal to 180°) at the fixed positions of other atoms.[5] In such a reaction with the linear symmetric transition state, this motion of the hydrogen atom coincides sufficiently well with the normal vibration Q with an imaginary frequency for the transition state

$$Q = \Delta x_H, \qquad (10)$$

since the corresponding displacements of the adjacent C atoms are small. It is clear that precisely this normal vibration coincides with the reaction coordinate in the transition state vicinity but further deviates from it on moving toward the reactants or products.

In the general case of the nonsymmetric linear transition state A—H—B, the normal vibration with an imaginary frequency includes motions of all groups of atoms

$$Q = \alpha\Delta x_A + \sqrt{1 - \alpha^2 - \beta^2}\,\Delta x_H + \beta\Delta x_B, \qquad (11)$$

and depending on the ratio of masses, the coefficients at the Δx displacements can be comparable for H, A, and B. The internal arrangement of the atoms in the polyatomic A and B groups changes to result in their structural relaxation, but we believe for simplicity that A and B move as a whole.

This pattern can be conformed to IPM if one strictly follows the concepts that the intersecting parabolic curves describe the energy of the A—H and H—B systems only depending on the elongation of the corresponding bonds.* In fact, if we designate the displacement along the approximate reaction coordinate (11)

* This interpretation, unlike the "straightforward" interpretation of intersecting parabolas as potential curves describing the interaction of the H atom with the fixed A and B groups, can also be applied to the case of the model representation of a change in the energy of the system along the true and complicated reaction coordinates.

Table 4. Total energy (E) including the zero-point energy ZPE and geometric characteristics of the reactants and transition states calculated by the B3LYP/6-311++G**, MP4/6-311++G**, and CCSD/6-311++G** methods

System	E+ZPE/hartree	Geometric characteristics				E_a^*/kJ mol^{-1}
		Bond	r/Å	Angle	ω/deg	
		B3LYP/6-311++G** method				
H—H*—H, TS	−1.66609	H*—H	0.9311	H—H*—H	180	14.9
H—H*—Cl, TS	−461.32941	H*—H	1.2764	H—H*—Cl	180	0.2 (H)
$C_{\infty v}$		Cl—H*	1.3448			18.3
H—H*—CH_3	−40.97852	H*—H	0.8907	H—H*—C	180	34.6 (H)
C_{3v}		C—H*	1.4148	H—C—H*	102.9	43.4
TS		C—H	1.0859			
H_3Si—H*—CH_3	−331.69752	H*—Si	1.6121	Si—H*—C	180	29.1 (CH_3)
C_{3v}		C—H*	1.6091	H—Si—H*	109.6	84.1
TS		C—H	1.0846	HC—H*	101.3	
		Si—H	1.4872	H—Si—C—H	60.0	
HO—H*—OH	−152.18964	H*—O	1.1655	H*—O—H	105.4	4.1
C_2, TS		O—H	0.9690	O—H*—O	146.0	
				H*—O—O—H	122.0	
HO—H*—OH	−152.18563	H*—O	1.1661	H*—O—H	101.3	18.3
C_s, TS		O—H	0.9685	O—H*—O	151.4	
				O—H*–O—H	69.4	
HO—H*—OH	−152.18482	H*—O	1.1623	H*—O—H	101.3	20.3
C_{2h}, TS2		O—H	0.9708	O—H*—O	180.0	
HO—H*—OH	−152.18642	H*—O	1.1616	H*—O—H	110.1	12.3
C_{2v}, TS3		O—H	0.9679	O—H*—O	162.0	
HO—H*—OH	−152.17081	H*—O	1.1448			56.0
$D_{\infty h}$, TS4		O—H	0.9564			
HOO—H*—OOH	−302.51104	H*—O	1.1829	H*—O—O	104.8	22.8
C_s, TS		O—O	1.3847	O—O—H	102.9	
		O—H	0.9710	O—H*—O	163.9	
				O—H*—O–O	87.3	
				H*—O–O—H	124.7	
HOO—H*—OOH	−302.51041	H*—O	1.1798	O—H*—O	180	24.4
C_i, TS2						
H_2N—H*—NH_2	−112.42018	H*—N	1.2496	H*—N–H	108.3	25.7
C_{2v}, TS		H—N	1.0221	N—H*—N	157.1	
				H—N–N—H	114.1	
H_2N—H*—NH_2	−112.41520	H*—N	1.2541	H*—N—H	100.6	38.8
C_{2h}, TS2		H—N	1.0257	H—N—H	103.8	
HH, $D_{\infty h}$	−1.16950	H—H	0.744			
HCl, $C_{\infty v}$	−460.82735	H—Cl	1.2869			
HOH, C_{2v}	−76.43725	H—O	0.9621	H—O—H	105.0	
NH_3, C_{3v}	−56.54847	H—N	1.014	H—N—H	107.9	
HOOH, C_2	−151.57573	H—O	0.9672	H—O—O	100.5	
		O—O	1.4541	H—O—O—H	121.4	
CH_4, T_d	−40.48942	C—H	1.0909	H—C—H	109.5	
SiH_4, T_d	−291.88308	Si—H	1.4839	H—Si—H	109.5	
H	−0.50226					
Cl	−460.16688					
HO	−75.75396	H—O	0.9759			
HOO, C_s	−150.94399	H—O	0.9771	H—O—O	105.9	
		O—O	1.3284			
NH_2, C_{2v}	−55.88150	H—N	1.0295	H—N—H	103.1	
CH_3, D_{3h}	−39.82554	H—C	1.0805	H—C—H	120	
SiH_3, C_{3v}	−291.24013	H—Si	1.4860	H—Si—H	111.1	
SiH_3, D_{3h}, TS	−291.23337	H—Si	1.4703	H—S—H	120	17.7

(*to be continued*)

Table 4 (*continued*)

System	*E*+ZPE/hartree	Geometric characteristics				E_a^*/kJ mol^{-1}
		Bond	*r*/Å	Angle	ω/deg	
			MP4/6-311++G** method			
H—H*—Cl, TS	−460.74569	H*—H	0.9798	H—H*—Cl	180	29.0 (H)
$C_{\infty v}$		Cl—H*	1.4234			41.2
HO—H*—OH	−151.83102	H*—O	1.1504	H*—O—H	102.9	56.8
C_2		O—H	0.9686	O—H*—O	144.1	
				H*—O–O—H	121.0	
HO—H*—OH	−151.83165	H*—O	1.1479	H*—O—H	98.3	55.2
C_{2h}, TS2		O—H	0.9705			
HO—H*—OH	−151.82905	H*—O	1.1502	H*—O—H	106.4	62.0
C_{2v}, TS2		O—H	0.9682	O—H*—O	161.4	
HO—H*—OH	−151.77255	H—O	1.1348			210.4
$D_{\infty h}$, TS4		O—H	0.9559			
HH, $D_{\infty h}$	−1.15762	H—H	0.7420			
HCl, $C_{\infty v}$	−460.263844	H—Cl	1.2746			
HOH, C_{2v}	−76.286570	H—O	0.9609	H—O—H	103.3	
H	−0.49982					
Cl	−459.60377					
HO, $C_{\infty v}$	−75.58697	H—O	0.9716			
			CCSD/6-311++G** method			
H—H*—Cl, TS	−460.74424	H*—H	1.0066	H—H*—Cl	180	26.2 (H)
$C_{\infty v}$		Cl—H*	1.4157			44.2
H—H*—Cl, TS	−460.74807	H*—H	1.0043	H—H*—Cl	180	24.3 (H)
$C_{\infty v}$(CCSD-T)		Cl—H*	1.4184			38.5
HO—H*—OH	−151.82351	H*—O	1.1566	H*—O—H	102.3	54.0
C_2, TS		O—H	0.9660	O—H*—O	145.5	
				H*—O–O—H	122.8	
HO—H*—OH	−151.82052	H*—O	1.1546	H*—O—H	98.4	61.8
C_{2h}, TS2		O—H	0.9676			
HO—H*—OH	−151.82074	H*—O	1.1556	H*—O—H	106.0	61.3
C_{2v}, TS3		O—H	0.9655	O—H*—O	162.7	
HO—H*—OH	−151.81932	H*—O	1.1570	H*—O—H	105.4	65.3
C_s, TS3		O—H	0.9655	O—H*—O	152.7	
				H—O–H*—O	62.0	
HO—H*—OH	−151.76528	H*—O	1.1312			206.3
$D_{\infty h}$, TS4		O—H	0.9530			
HH, $D_{\infty h}$	−1.15830	H—H	0.7435			
HCl, $C_{\infty v}$	−460.25435	H—Cl	1.2762			
HCl, $C_{\infty v}$ (CCSD-T)	−460.25751	H—Cl	1.2777			
HOH, C_{2v}	−76.25952	H—O	0.9584	H—O—H	103.6	
H	−0.49982					
Cl	−459.60276					
Cl (CCSD-T)	−459.60443					
HO, $C_{\infty v}$	−75.58455	H—O	0.9708			

* For reactions with the nonsymmetric transition state for one of the channels, the reactant for assignment of the activation energy is indicated in parentheses.

as q, the positions of A, H, and B in the A—H—B axis are described by the functions

$$A(q) = -r_{A-H} + \alpha q,$$
$$H(q) = q\sqrt{1 - \alpha^2 - \beta^2}, \quad (12)$$
$$B(q) = r_{B-H} + \beta q.$$

To conserve the correct total energies of the reactants and products, one has to consider that the internal geometry of the A and B fragments is the same as that in the AH and HB molecules. Then the square relations for the potential energies of the AH and HB subsystems follow from (12)

$$U_{AH} = -D_{AH} + b^2[r_{AH} + (A(q) - H(q))]^2,$$
$$U_{BH} = -D_{BH} + (b_f)^2[r_{BH} + (B(q) - H(q))]^2. \quad (13)$$

When the current distance A—H and B—H, respectively, is chosen instead of q as an independent variable in (13), we obtain the canonical expressions for (1) and (2) for IPM.

This result can be seen in Fig. 1 where the positions of the A, H, and B atoms are indicated by the dotted line for the simplified reaction coordinate (q), and the bold line shows them for the true reaction coordinate Q (11). It is clear that a more complicated concerted motion of the A, H, and B atoms does not change the key points in the energy scale for the initial, transition, and final states and the elongation of the A—H and H—B bonds in the transition state with respect to their equilibrium values.

The cross sections of the potential energy surfaces in the vicinity of the transition state calculated according to (11) for the H—H—H, H—H—Cl, H—H—CH_3, and H_3C—H—SiH_3 systems are presented in Fig. 2. Naturally, these cross sections possess maximum points in the transition state, unlike the cross sections calculated for the H atom displacements at the fixed positions of other atoms (for example, for the H—H—Cl system, a minimum in the transition state takes place in this case). These cross sections also possess two minima, and the corresponding A—H or H—B distance for each of them coincides satisfactorily with its equilibrium value (Table 5).

This is likely resulted from the fact that the energy increases strongly for the A—H and H—B distances, which are shorter than their equilibrium values. However, the depths of these minima are small, as a rule, compared to a change in the energy along the true coordinate of the H atom transfer reaction with the complete structural relaxation of the A and B fragments. The main reason for the slight energy change along the calculated cross sections is that the AH and B, A and HB systems very tightly contact in the minimum points at the H...B and A....H distances, which are much shorter than the sum of the corresponding van der Waals radii, and this contact results in an additional increase in the energy.

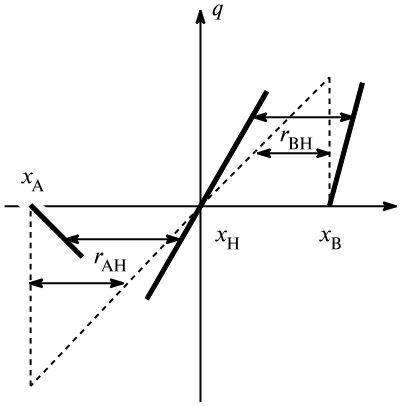

Fig. 1. Positions of the H atom and atomic groups A and B as functions of the reaction coordinate (q) in different models of passing through the transition state by the system: dotted line, only the H atom displaces; and bold lines, all atoms displace according to the normal vibration shape with an imaginary frequency in the transition state. Equilibrium distances are shown by arrows.

Based on these observations, it seems reasonable to present the following simplified model for estimation of the transition state. The model qualitatively corresponds to the intersecting parabolas and intersecting Morse curves methods and is based on the assumption that for the reaction

$$B^{\bullet} + HA \longrightarrow BH + A^{\bullet}$$

before the transition state is achieved, the interaction of AH and $B^{\bullet}$ and, after passing the transition state, the interaction of $A^{\bullet}$ and BH are considered switched-off. As mentioned above, to retain the correct total energies of the reactants and products, the elongation of the A—H and H—B bonds should necessarily be performed at the fixed geometry of the A and B fragments. Thus, the effects of structural relaxation of A and B during the reaction are ignored. However, they are not very significant because of the softness of angular deformation vibrations due to which this relaxation mainly occurs.

Table 5. Characteristic of positions of minima Δr_{A-H} and Δr_{B-H} on the potential energy cross sections in the vicinity of the transition state (distances are given in Å)

A—H—B system	Δr_{A-H}	$r_{A-H} - r_{AH}$	Δr_{B-H}	$r_{B-H} - r_{BH}$	$\Delta r_{A-H} + \Delta r_{B-H}$
H—H—H	0.07	0.12	—	—	0.14
H—H—Cl	0.37	0.10	0.05	0.10	0.42
H—H—CH_3	0.09	0.06	0.22	0.09	0.31
SiH_3—H—CH_3	0.05	0.07	0.49	0.03	0.54
HO—H—OH	0.19	0.01	—	—	0.38
HOO—H—OOH	0.18	0.03	—	—	0.36
H_2N—H—NH_2	0.18	0.04	—	—	0.36

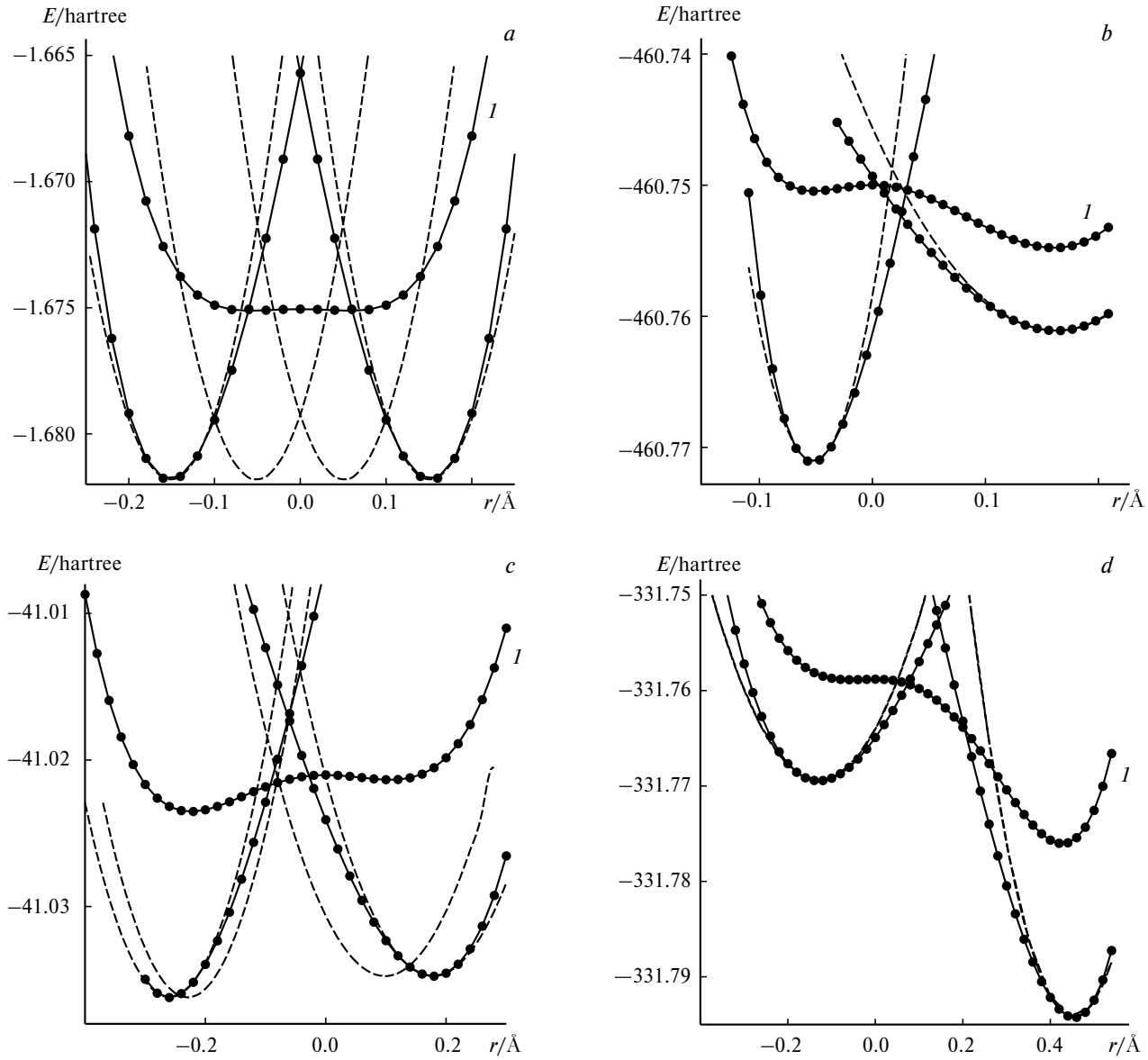

Fig. 2. Cross sections of the potential energy surface (E) of the H—H—H (*a*), H—H—Cl (*b*), CH_3—H—H (*c*), and CH_3—H—SiH_3 (*d*) systems in the vicinity of the transition state as functions of the displacement (r) along the normal vibration with an imaginary frequency (curve *1*). The energies of the reactants and products for the corresponding elongations of the reacting bond lengths are marked by solid intersecting curves, and their parabolic approximations are shown by dotted curves.

The total energies of the system calculated in this approximation are shown in Fig. 2 as solid intersecting curves. The parabolic approximations of these curves are shown by dotted lines. It is seen that the points of their intersection are sufficiently well localized in the vicinity of transition states. Ignoring the structural relaxation of A and B can efficiently be corrected if the terms describing the reactants and products are shifted toward each other by a short distance (this to a less extent changes the geometric characteristics of the point of their intersection). As an example for the $H^{\bullet} + H_2$ system, the parabolic approximations of the H_2 terms are shifted by 0.12 Å in such a way that the positions of their minima coincide with the positions of minima of the potential energy cross sections for the $H^{\bullet} + H_2$ system (see Fig. 2, *a*).* Then the point of their intersection is located lower than the energy barrier of the reaction. This sensitivity of the position of the intersection point to the sum of the r_{A-H} and r_{H-B} distances allows the r_e distance to be used as the effective empirical parameter in the *a priori* estimation of experimental activation energies in the framework of IPM.

* In the case of the H—H—CH_3 system, the use of positions of minima on the cross section of the potential energy surface for the estimation of displacements of parabolic terms makes it possible to estimate the energy barrier with a high accuracy (see Fig. 2). However, in the case of early or late transition states, this approach can give a much lower accuracy.

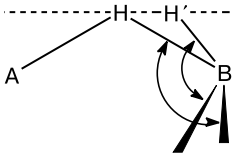

Fig. 3. Scheme of the turn of fragment B matched with the motion of the H atom in such a way that the H—B and H′—B directions coincide in the internal system of coordinates.

For nonlinear symmetric transition states in the $HO^{\bullet}$ + HOH, $HOO^{\bullet}$ + HOOH, and $H_2N^{\bullet}$ + HNH_2 systems, the reaction coordinate corresponds to the motion of the H atom not along the formed or cleaved bond but at some angle to these bonds. In this case, the calculation of the cross sections in the framework of the simplified model corresponds to the rotation of the A or B group concerted with the H displacement (Fig. 3). A similar assumption should also be accepted for IPM. The thus calculated total energies of the deformed reactants and products are shown in Fig. 4 by solid intersecting curves, and their parabolic approximations are shown by dotted curves.

Comparison of calculation results

The interatomic distances in the reaction site of the transition state calculated by different methods are collected in Table 6.

The comparison of the interatomic distances calculated by the quantum-chemical methods (QCH) and from the experimental data using the IPM method shows that they are close, as a rule, and r(QCH) > r(IPM). The statistical processing of these data using the least-squares method gives the following correlation between the A—H and B—H interatomic distances in the A...H...B transition state:

$$r(\text{IPM}) = r(\text{QCH}) - (0.45 \pm 1.14) \cdot 10^{-11} \text{ m}. \qquad (14)$$

The difference between r(IPM) and r(QCH) is only $\Delta r = 4.5 \cdot 10^{-12}$ m and is lower than the root-mean-square error in the estimation of the difference between these values equal to $11.4 \cdot 10^{-12}$ m. Thus, the estimation of the parabolic model of interatomic distances in the transitions state is rather similar to that of the quantum-chemical calculations. The r values in the IPM model are still closer to r(QCH)

$$r(\text{IMM}) = r(\text{QCH}) + (0.19 \pm 1.10) \cdot 10^{-11} \text{ m}. \qquad (15)$$

In this case, the mean divergence between the Δr ($1.9 \cdot 10^{-12}$ m) values is fivefold lower than the root-mean-square error ($11.4 \cdot 10^{-12}$ m).

The r_{A-B} distance is an important characteristic of the A...H...B transition state. In the quantum-chemical calculation $r_{A-B} = r_{A-H} + r_{B-H}$, and in the IPM and IMM models $r_{A-B} = r_{AH} + r_{BH} + r_e$. Let us compare r_{A-B}

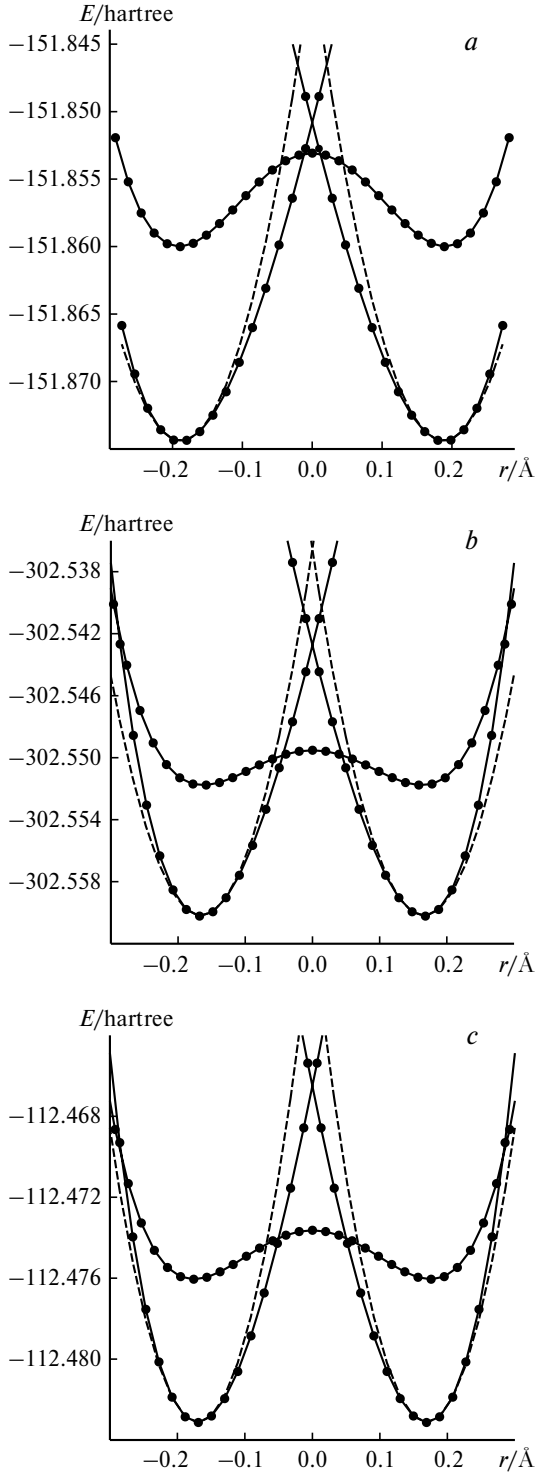

Fig. 4. Cross sections of the potential energy surface (E) for the HO—H—OH (*a*), HOO—H—OOH (*b*), and NH_2—H—NH_2 (*c*) systems in the vicinity of the transition state as functions of the displacement R along the normal vibration with an imaginary frequency (upper curve). The energies of the reactants and products for the corresponding elongations of the reacting bond lengths are shown by solid intersecting curves, and their parabolic approximations are shown by dotted curves.

Table 6. Interatomic distances in the transition state calculated by the quantum-chemical (QCH), IPM, and IMM methods (distances are given in m)

Reaction	Bond	QCH	IPM		IMM	
		$r \cdot 10^{11}$	$r \cdot 10^{11}$	$\Delta r \cdot 10^{11}$	$r \cdot 10^{11}$	$\Delta r \cdot 10^{11}$
$H^{\cdot} + H_2$	H—H [a]	9.31	9.23	0.08	9.63	−0.32
$H^{\cdot} + HCl$	H—Cl [b]	14.16	14.16	0.00	14.39	−0.23
$H^{\cdot} + HCl$	H—H [b]	10.07	9.06	1.01	9.37	0.70
$H^{\cdot} + CH_4$	C—H [a]	14.15	12.86	1.29	13.48	0.67
$H^{\cdot} + CH_4$	H—H [a]	8.91	9.57	−0.66	10.18	−1.27
$C^{\cdot}H_3 + CH_4$ [c]	C—H [a]	13.53	13.00	0.53	13.55	−0.02
$N^{\cdot}H_2 + NH_3$	N—H [a]	12.50	12.18	0.32	12.80	−0.30
$HO^{\cdot} + H_2O$	O—H [b]	11.57	10.90	0.67	12.80	−1.23
$C^{\cdot}H_3 + SiH_4$	Si—H [a]	16.12	18.02	−1.90	18.49	−2.37
$C^{\cdot}H_3 + SiH_4$	C—H [a]	16.09	13.17	2.92	14.14	1.95
$HO_2^{\cdot} + H_2O_2$	O—H [a]	11.83	11.13	0.70	11.43	0.40

[a] B3LYP/6-311++G** method.
[b] CCSD/6-311++G** method.
[c] According to the data in Ref. 30.

obtained by the quantum-chemical and IPM calculations (Table 7).

The statistical processing of the obtained r_{A-B} values gives the following correlation between the $r_{A-B,}$ values calculated using different methods:

$$r_{A-B}(IPM) = r_{A-B}(QCH) - (0.70 \pm 0.55) \cdot 10^{-11} \text{ m} \quad (16)$$

In this case, we can see a systematic difference between r_{A-B}(QCH) and r_{A-B}(IPM): $\Delta r_{AB} = 7 \cdot 10^{-12}$ m is 1.5 times larger than the root-mean-square error ($5.5 \cdot 10^{-12}$ m). It is substantial that this error is much lower, as a rule, than the difference in the r_{A-H-B} distances for reactions of different classes. Based on this fact, the geometry of the transition state can rather reliably be estimated from the empirical parameter r_e. In the IPM method, the source of scatter of the data (values of the r_e parameter) is the data scatter over the activation energies measured using different methods and by different authors (see formula (3) for estimation of r_e). According to the data presented in Table 7, the root-mean-square error in the estimation of r_{A-B} by the IPM method is only $0.94 \cdot 10^{-12}$ m. Therefore, the total error (data scatter) in the estimation of r_{A-B} follows mainly from the effective character of the r_e value determined from the experimental data and dependent on different aspects of the reaction. It is most likely that the data scatter is mainly affected by the factor of the nature of the transition state (early or late), which changes the activation energy at the same total bond elongation in the saddle point. In particular, this is seen from the fact that the scatter of the r_{A-B} values is twofold lower than the scatter of the r_{A-H} and r_{B-H} values.

Table 7. Comparison of the r_{A-B} distances calculated by the quantum-chemical methods and IPM method

Reaction	Distance	$r_{A-B} \cdot 10^{11}$/m		$\Delta r \cdot 10^{11}$/m
		IPM	QCH	
$H^{\cdot} + H_2$	H—H—H	18.46±0.08	18.62 [a]	0.16
$H^{\cdot} + HCl$	H—H—Cl	23.22±0.01	24.22 [b]	1.00
$H^{\cdot} + CH_4$	H—H—C	22.43±0.15	23.05 [a]	0.62
$C^{\cdot}H_3 + CH_4$	C—H—C	26.00±0.13	26.94 [c]	0.94
$C_2H_5^{\cdot} + C_2H_6$	C—H—C	26.00	27.06 [d]	1.06
$N^{\cdot}H_2 + NH_3$	N—H—N	24.36	24.99 [a]	0.63
$HO^{\cdot} + HOH$	O—H—O	21.80	21.23 [b]	0.57
$HO_2^{\cdot} + HOOH$	O—H—O	22.26±0.10	23.66 [a]	1.40
$C^{\cdot}H_3 + SiH_4$	C—H—Si	31.19	32.21 [a]	1.02

[a] B3LYP/6-311++G(d,p) calculation, this work.
[b] CCSD/6-311++G(d,p) calculation, this work.
[c] B3LYP/6-311+G(d,p) calculation.[30]
[d] B3LYP/6-311++G(d,p) calculation.[5]

The use of different quantum-chemical methods slightly affects the transition state geometry (see Table 4) but has a noticeable influence on the activation energy, as it has been mentioned above. The experimental activation energies for the B + HA reaction and those calculated by the density functional or coupled clusters methods are presented in Table 8.

As can be seen from the data in Table 8, the sufficiently satisfactory correspondence between the quantum-chemically calculated and experimental E_a values is observed for all cases except the $HO^{\bullet} + H_2O$ system. The coincidence of the calculated and experimental results is almost complete for the $HO_2^{\bullet} + HOOH$ and $C^{\bullet}H_3 + SiH_4$ reactions. For the $H^{\bullet} + HCl$ and $HO^{\bullet} + H_2O$ systems, the use of the coupled clusters method qualitatively improves the agreement with experiment, although gives

Table 8. Comparison of the experimental activation energies for some reactions and those calculated by the density functional or coupled clusters methods

Reaction	E_a/kJ mol^{-1}	
	Experiment	Calculation
$H^{\cdot} + H_2$	29.0 ± 2.4	14.9
$H^{\cdot} + HCl$	14.5 ± 0.5	26.2*
$H^{\cdot} + CH_4$	56.0 ± 5.2	34.6
$C^{\cdot}H_3 + CH_4$	58.6 ± 4.2	46.1
$N^{\cdot}H_2 + NH_3$	61.3	38.8
$HO^{\cdot} + H_2O$	18.4	54.0*
$HO_2^{\cdot} + HOOH$	23.1	22.8
$C^{\cdot}H_3 + SiH_4$**	29.4	29.1

* Calculated by the coupled clusters method.
** According to the data in Ref. 30.

overestimated activation barriers. As for the absolute error of determination of the activation energy, it remains virtually unchanged for the first system and increases by 2.5 times for the second system despite a considerable increase in time expenses for calculations.

Thus, the interatomic distances in the transition state, which can be calculated using the IPM and IMM models from experimental data (E, ΔH) for radical abstraction reactions are rather close to those calculated by the density functional method. The simple correlation of the $r_{A-H}(QCH) = a + r_{A-H}(IPM)$ type can be used for the approximate estimation of the interatomic distances in the transition state using experimental data (formulas (3)—(6)).

References

1. E. T. Denisov, *Kinet. Katal.*, 1991, **32**, 461 [*Kinet. Catal.*, 1991, **32**, 406 (Engl. Transl.)].
2. E. T. Denisov, *Mendeleev Commun*, 1992, **2**, 1.
3. E. T. Denisov, *Usp. Khim.*, 1997, **66**, 953 [*Russ. Chem. Rev.*, 1997, **66**, 859 (Engl. Transl.)].
4. E. T. Denisov and V. V. Tumanov, *Zh. Fiz. Khim.*, 1994, **68**, 719 [*Russ. J. Phys. Chem.*, 1994, **68**, 645 (Engl. Transl.)].
5. A. F. Shestakov, T. G. Denisova, E. T. Denisov, and N. S. Emel´yanova, *Izv. Akad. Nauk, Ser. Khim.*, 2002, 602 [*Russ. Chem. Bull., Int. Ed.*, 2002, **51**, 559].
6. M. J. Frisch, G. W. Trucks, M. Head-Gordon, P. M. W. Gill, M. W. Wong, J. B. Foresman, B. G. Johnson, H. B. Schlegel, M. A. Robb, E. S. Replogle, R. Gomperts, J. L. Andres, K. Raghavachari, J. S. Binkley, C. Gonzalez, R. L. Martin, D. J. Fox, D. J. Defrees, J. Baker, J. J. P. Stewart, and J. A. Pople, *GAUSSIAN 98, Revision A 6*, Gaussian Inc. Pittsburgh PA, 1998.
7. *Handbook of Chemistry and Physics*, Ed. D. Lide, CRC Press, Boca Raton, 1992.
8. M. J. Cohen, A. Willets, and N. C. Handy, *J. Chem. Phys.* 1993, **99**, 5885.
9. M. J. Cohen, N. C. Handy, R. Hernandez, and W. H. Milles, *Chem. Phys. Lett.*, 1992, **192**, 407.
10. B. C. Garrett, D. G. Trular, and G. C. Schatz, *J. Am. Chem. Soc.*, 1986, **108**, 2876.
11. G. Leroy, N. Sana, and A. Tinant, *Can. J. Chem.*, 1985, **63**, 1447.
12. M. van Meersche, *Bull. Soc. Chim. Belg.*, 1951, **60**, 99.
13. T. C. Allison, G. C. Linch, D. G. Truhlar, and M. S. Gordon, *J. Phys. Chem.*, 1996, **100**, 13575.
14. D. Kita and D. H. Stedman, *J. Chem. Soc., Faraday Trans. 2*, 1982, **78**, 1249.
15. J. C. Miller and R. J. Gordon, *J. Chem. Phys.*, 1981, **75**, 5305.
16. D. L. Baulch, J. Duxbury, S. J. Grant, and D. C. Montague, *J. Phys. Chem. Ref. Data*, 1981, **10**, Suppl.
17. P. F. Ambidge, J. N. Bradley, and D. A. Whytock, *J. Chem. Soc., Faraday Trans. 1*, 1976, **72**, 2143.
18. J. Espinoza-Garcia and J. C. Corchado, *J. Phys. Chem.*, 1996, **100**, 16561.
19. H. J. Baeck, K. S. Shin, H. Yang, Z. Qin, V. Lissaki, and W. C. Gardiner, *J. Phys. Chem.*, 1995, **99**, 15925.
20. P.-M. Marquaire, A. G. Dastidar, and P. D. Pacey, *Can. J. Chem.*, 1994, **72**, 600.
21. D. L. Baulch, C. J. Cobos, R. A. Cox, C. Esser, P. Frank, Th. Just, J. A. Kerr, M. J. Pilling, J. Troe, R. W. Walker, and J. Warnatz, *J. Phys. Chem. Ref. Data*, 1992, **21**, 411.
22. M. J. Rabinovitz, J. W. Sutherland, P. M. Patterson, and R. B. Klemm, *J. Phys. Chem.*, 1991, **95**, 674.
23. N. L. Arthur and T. N. Bell, *Rev. Chem. Intermed.*, 1978, **2**, 37.
24. F. S. Dainton, K. J. Ivin, and F. Wilkinson, *Trans. Faraday Soc.*, 1959, **55**, 929.
25. M. K. Dubey, R. Mohrschladt, N. M. Donahue, and J. G. Anderson, *J. Phys. Chem.*, 1997, **101**, 1494.
26. R. E. Berkley, I. Safaric, O. P. Strausz, and H. E. Grenning, *J. Phys. Chem.*, 1973, **77**, 1741.
27. H. E. O´Neal, S. Pavlou, T. Lubin, M. A. Ring, and L. Batt, *J. Phys. Chem.*, 1971, **75**, 3945.
28. O. P. Strausz, E. Jakubowski, H. S. Sandhu, and H. E. Gunning, *J. Chem. Phys.*, 1969, **51**, 552.
29. E. R. Morris and J. C. J. Thynne, *J. Phys. Chem.*, 1969, **73**, 3294.
30 S. Skokov and R. A. Wheeler, *Chem. Phys. Lett.*, 1997, **271**, 251.
31. B. S. Jursic, *J. Mol. Struct. (Theochem.)*, 1998, **428**, 49.
32. B. S. Jursic, *J. Mol. Struct. (Theochem.)*, 1998, **427**, 137.
33. B. J. Lynch and D. G. Truhlar, *J. Phys. Chem. A*, 2001, **105**, 2936.

Received July 6, 2002